ACS OMEGA

http://pubs.acs.org/journal/acsodf

Article

Effect of Electron and Proton Irradiation on Structural and Electronic Properties of Carbon Nanowalls

Yerassyl Yerlanuly, Rakhymzhan Ye Zhumadilov, Igor V. Danko, Daniyar M. Janseitov, Renata R. Nemkayeva, Alexander V. Kireyev, Aidana B. Arystan, Gulnur Akhtanova, Joachim Vollbrecht, Nora Schopp, Aliya Nurmukhanbetova, Tlekkabul S. Ramazanov, Askhat N. Jumabekov, Pavel A. Oreshkin, Timur K. Zholdybayev, Maratbek T. Gabdullin,* and Viktor V. Brus*

Cite This: *ACS Omega* 2022, 7, 48467−48475

Read Online

ACCESS | Metrics & More | Article Recommendations

ABSTRACT: In this work, a complex experimental study of the effect of electron and proton ionizing radiation on the properties of carbon nanowalls (CNWs) is carried out using various state-of-the-art materials characterization techniques. CNW layers on quartz substrates were exposed to 5 MeV electron and 1.8 MeV proton irradiation with accumulated fluences of 7×10^{13} e/cm^2 and 10^{12} p/cm^2, respectively. It is found that depending on the type of irradiation (electron or proton), the morphology and structural properties of CNWs change; in particular, the wall density decreases, and the sp^2 hybridization component increases. The morphological and structural changes in turn lead to changes in the electronic, optical, and electrical characteristics of the material, in particular, change in the work function, improvement in optical transmission, an increase in the surface resistance, and a decrease in the specific conductivity of the CNW films. Lastly, this study highlights the potential of CNWs as nanostructured functional materials for novel high-performance radiation-resistant electronic and optoelectronic devices.

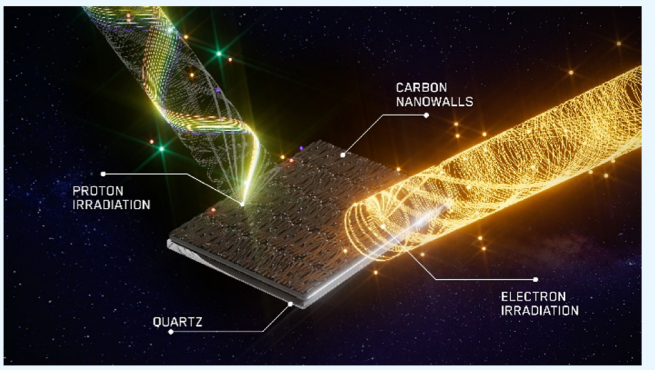

INTRODUCTION

A prolonged exposure to ionizing radiation damages and ultimately destroys functional semiconductor materials in electronic devices, limiting their lifetime.[1−3] Irradiation exposure can cause chemical bonds within a material to break, altering their morphological and structural characteristics, which in turn can cause it to swell, polymerize, cause corrosion, cause quality loss, contribute to cracking, or otherwise change its desired mechanical, optical, or electronic properties.[1−12] Achieving high stability under intense ionizing irradiation is of great importance for many applications, ranging from nuclear power reactors to electronics for the emerging space industry. Satellites orbiting the Earth experience both electron and proton bombardment.[4−7] As scientific and commercial space missions have rapidly become more and more ambitious, the employed functional electronic materials have to meet growing requirements for their radiation resistance as well. A reliable operation in extreme environments with different types of ionizing radiation is a crucial prerequisite for the success of such missions. In light of these materials science challenges, extensive research of novel radiation-resistant materials takes place alongside efforts to gain an in-depth understanding of the radiation-induced processes and how to mitigate them.[2,8−12]

Various allotropic modifications of carbon and a wide range of their practical applications[13−16] are attracting increasing attention in the field of radiation-resistant electronics and optoelectronics.[9,17−22] Currently, experimental works on the irradiation of carbon nanostructures focus on the induced changes in mechanical, electronic, and even magnetic properties.[8,23,24] There are also several experimental studies of the radiation resistance of carbon nanomaterials and devices based on them.[21,25] Narayan et al.[21] irradiated Q-carbon with heavy ions, inducing extreme atomic displacements and electronic excitations. Studies of samples before and after ion irradiation reveal that the atomic structure and bonding characteristics of the Q-carbon sample, as well as the sapphire substrate,

Received: October 19, 2022
Accepted: December 1, 2022
Published: December 12, 2022

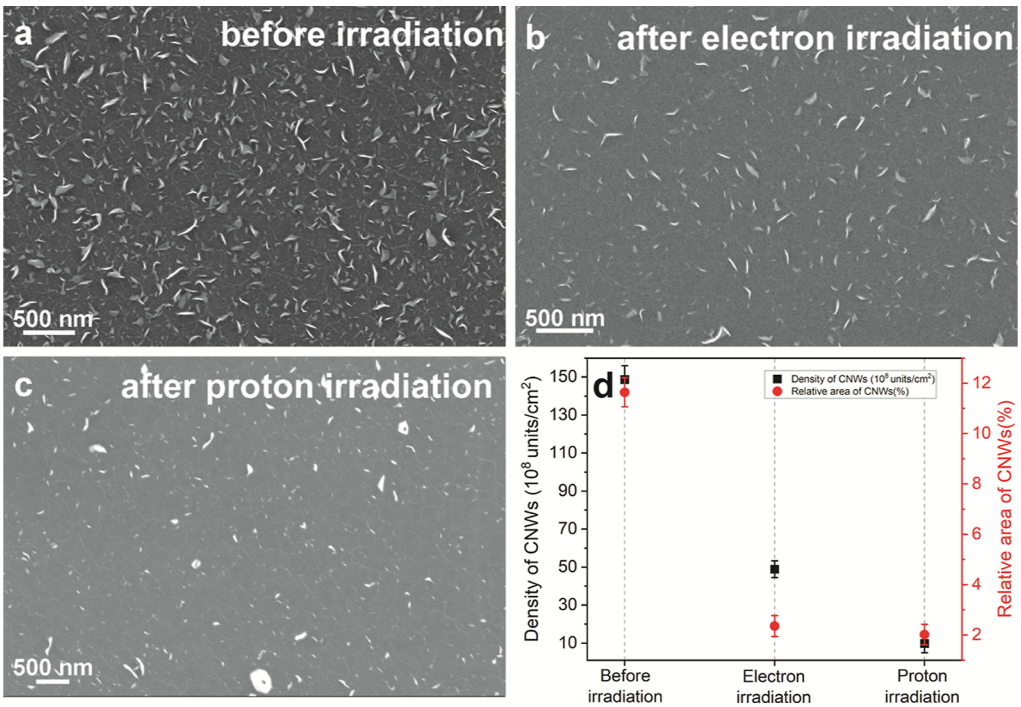

Figure 1. SEM images of CNW films (a) before, (b) after electron, and (c) after proton irradiation. (d) Changes in the density and relative area of CNWs before and after irradiation processes.

remained unchanged after irradiation with an accumulated dose of 10 dpa (displacements per atom), which is equivalent to more than 20 years of neutron exposure in a conventional nuclear reactor, suggesting excellent radiation-hardness. Kanhaiya et al.[3] investigated carbon nanotubes for radiation-resistant electronics. The authors have demonstrated radiation-tolerant carbon nanotube field-effect transistors (CNFETs) using both the extrinsic advantages of CNFETs due to the geometry of the devices provided by their low-temperature fabrication and the inherent properties of the carbon nanotube material. In summary, carbon nanomaterials are exceptionally promising as radiation-resistant functional electronic materials.

Over the past 2 decades, one of the widely studied allotropic modifications of carbon is so-called carbon nanowalls (CNWs). CNWs are three-dimensional networks with open edges connected by vertically oriented graphene nanosheets, which are freely arranged perpendicular to the substrates and form a labyrinth-like surface.[26,27] As compared to classic graphene, CNWs typically have a large specific surface area. At the same time, due to the vertical orientation of small graphene sheets, there is always a rather high level of defectiveness contributed by crystallite edges.[28,29] According to the literature, different morphological forms of CNWs have been observed depending on the arrangement of vertical graphene sheets, including petal-like, cauliflower-like, maze-like, or floc-like structures.[27,30,31] Owing to unique structural, morphological, electrical, optical, and chemical properties,[26,27,32,33] CNWs are attracting more attention as a functional electronic material for solar cells,[34−37] light-emitting diodes,[38,39] sensors,[40,41] superhydrophobic coatings,[42,43] and supercapacitors,[44,45] which have recently become more popular due to the ubiquity of wearable electronics and portable devices.[46,47] However, until today, there were only a few papers focused on the effect of ionizing radiation on the properties of CNWs.[48] For instance, Esquinazi et al.[48] studied the effect of proton irradiation on the magnetic properties of CNWs. The results suggest the existence of strong magnetic field gradients at some edges, indicating a ferromagnetic order in CNWs after proton irradiation. It was shown that proton irradiation might produce defects in the graphene layers of the walls, enhancing their magnetic order. Thus, considering the wide range of practical applications of CNWs and the urging demand for novel nanostructured radiation-resistant electronic materials, a systematic understanding of the effect of different ionizing radiations on the properties of CNWs is essential.

This contribution is devoted to the detailed study of the effect of electron and proton irradiation on the properties of CNWs, employing state-of-the-art materials characterization techniques. Morphological, structural, optical, and electrical properties of CNWs were rigorously investigated before and after an irradiation treatment with electrons and protons under controlled conditions.

RESULTS AND DISCUSSION

Figure 1 shows SEM images of CNW films on quartz substrates before and after electron and proton irradiation. Prior to irradiation, CNW films have a petal-like structure (Figure 1a). As shown in the SEM images, the morphology of the CNW films changes significantly after the irradiation process. After electron (Figure 1b) and proton (Figure 1c) irradiation, the density of CNWs decreases, resulting in separately standing (few-layer) graphene sheets. An analysis of the SEM images performed using ImageJ software is shown in Figure 1d; the resulting graphs demonstrate a decrease in density (units per cm^2) and relative area (%) of CNWs after the irradiation process.

Figure 2 shows the results of the structural analysis of the CNW films before and after the electron and proton irradiation treatments, obtained using Raman spectroscopy. The deconvolution of the Raman spectra was done according to the

https://doi.org/10.1021/acsomega.2c06735
ACS Omega 2022, 7, 48467−48475

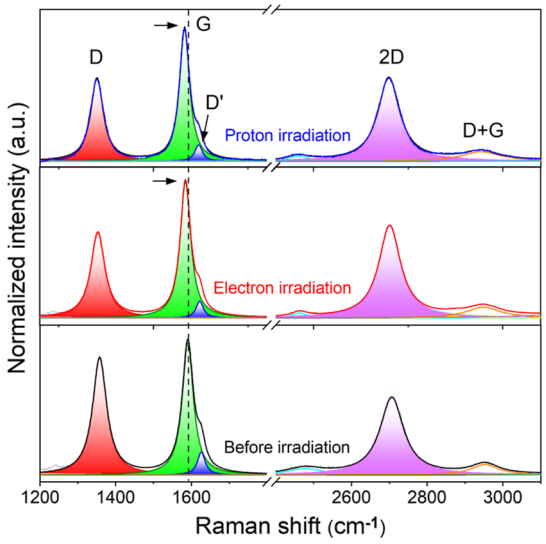

Figure 2. Raman spectra of the CNW films before and after electron and proton irradiation.

studies.[49,50] The CNW samples demonstrate typical Raman spectra with distinct characteristic graphite peaks D, G, D′, G′ (2D), and G + D.[30,51] The D band is associated with defects in sp^2 structures. Peak G is an inherent band of graphite materials. The shoulder D′ corresponds to the breaking of the symmetry in the sp^2 crystal of finite size and is characteristic of graphene edges. Peak G′ (2D) is the second order of the D mode. The appearance of this peak indicates a long-range order in the structure. The G + D (D″) peak is a band that arises from the combination of the G and D peaks. A detailed analysis of the Raman spectra is presented in Table 1. D and G peaks are red-

Table 1. Comparison of the Raman Spectrum Parameters of CNWs before and after Electron/Proton Irradiation

	before irradiation	electron irradiation	proton irradiation
D peak position (cm−1)	1357.8	1353.3	1350.4
G peak position (cm−1)	1590.6	1584.69	1581.9
D′ peak position (cm−1)	1626.3	1622.2	1619.7
2D peak position (cm−1)	2706	2701	2698.6
fwhm G (cm−1)	35.54	33.74	32.89
I(G)/I(D)	1.13	1.59	1.57
I(G)/I(D′)	5.77	8.24	8.77
I(2D)/I(G)	0.58	0.68	0.62

shifted after electron and proton irradiation with respect to their position in the as-prepared reference sample. The position of these peaks after proton irradiation is characteristic to graphene.[52] The analysis of the Raman spectra shows that the ratio of the intensities of the G and D peaks (I(G)/I(D)) increases after both electron and proton irradiation, which indicates a decrease in defects in the CNW structure. This may be due to the decreased density of CNWs after irradiation processes. The peak intensity ratio I(G)/I(D′) indicates the level of disorder in the graphite structures; after irradiation, the intensity of the D′ peak decreases, indicating a reduced number of vacancies in the sp^2 structure. The relative intensity of the 2D peak is usually used to estimate the number of graphene layers;[52] the peak ratio I(2D)/I(G) increases after irradiation, which indicates a decrease in the number of layers of graphene sheets (and a general increase in the order) in the resulting film. This phenomenon may be associated with possible swelling of the CNWs during irradiation[53] (and reduction of defective areas). In addition, the relative number of defects in the structure of CNW films can be assessed by the full width at half maximum (fwhm) of the G peak. It is observed that the electron and proton irradiation treatments lead to a decrease in fwhm (G), which corresponds to a lower defect density. The decrease in defects in CNWs after irradiation can be explained by the lower density of vertically oriented graphene sheets (Figure 1).

X-ray photoelectron spectroscopy (XPS) measurements of the samples were carried out to inspect chemical bonds in the CNW films before and after electron and proton irradiation. Figure 3a shows the XPS spectra of the CNW film before and after irradiation. The spectra reveal a pronounced, intense carbon peak, as well as peaks of silicon oxide (substrate material). It can be seen that after electron and proton irradiation, the intensity of the carbon peak decreases, while the intensity of the silicon oxide peak increases. This trend is associated with a decrease in the density of CNWs on the substrate surface after the irradiation process (see Figure 1). Figures 3b–d show the XPS spectra of the carbon region (C 1s) fitted using the Gauss approximation for the samples before and after electron and proton irradiation, respectively. Before the deconvolution of XPS spectra, the background signal was subtracted by the standard Shirley method using Origin software. As can be seen from the spectra, the C 1s peak consists mainly of the following peaks: a peak at 284.5 eV that corresponds to the sp^2 hybridization characteristic of the double (C═C) carbon bond[54] and a peak at 285.4 eV that corresponds to the sp^3 hybridization characteristic of either a single (C−C) carbon bond or a (C−H) hydrocarbon bond.[55,56] Peaks at 286.4 and 290.7 eV indicate the existence of hydroxyl (C−OH) and carboxyl (O═C−OH) groups on the surface of CNWs, respectively.[54] These peaks can be caused by traces of precursors (H_2 and CH_4) and residual oxygen in the vacuum chamber during the synthesis. Molecules of oxygen and hydrogen can also adsorb onto CNWs from the atmosphere after synthesis due to the partially turbostratic nature of the structure with a high specific surface area and chemically active dangling bonds. It is noteworthy that after the electron and proton bombardments, the spectra clearly show a peak at 288.6 eV, which corresponds to the carboxylate (O−C═O^- or $RCOO^-$) group.[57] This is most likely due to the fact that after the irradiation process, carboxyl (O═C−OH) groups change into carboxylate O−C═O− groups.[58] This factor can also affect (induce) the increase in sp^3 hybridization.

The deconvoluted XPS spectra in the region of the C 1s peak, as shown in Figure 3, revealed different types of carbon bonds. The total contribution of each type of carbon bond is summarized in Table 2. These results indicate that the samples after both electron and proton irradiation demonstrate similar behavior, showing the presence of carboxylate O−C═O^- groups. It is noteworthy that after the irradiation treatments, the ratio of C═C peaks to the total area (of the carbon peak) increases, which also indicates an increase in sp^2 hybridization content and is consistent with the results of the Raman analysis.

https://doi.org/10.1021/acsomega.2c06735
ACS Omega 2022, 7, 48467−48475

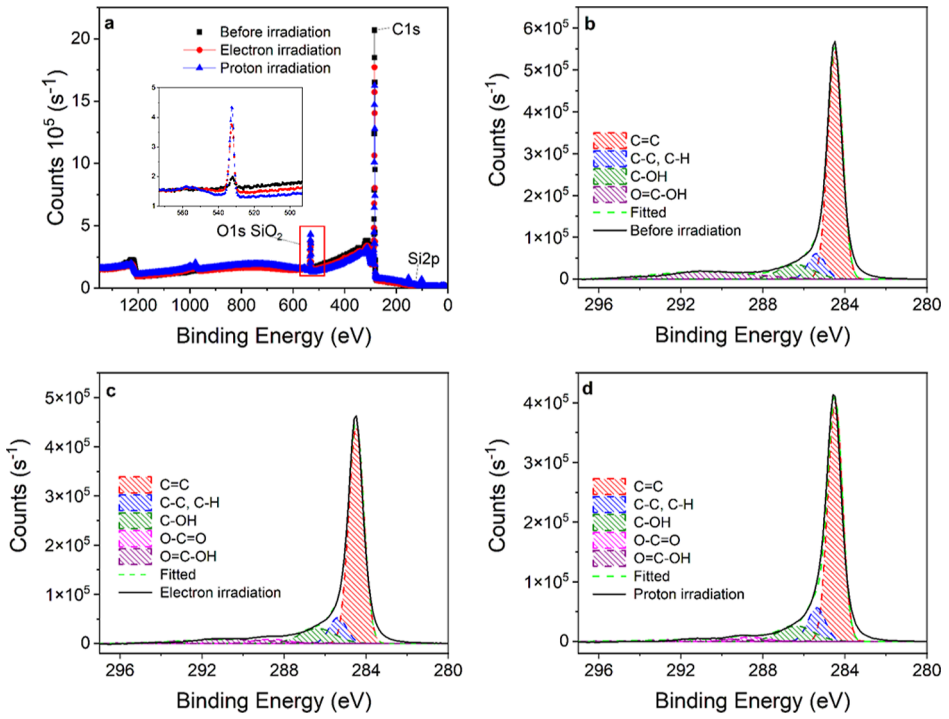

Figure 3. XPS analysis of the CNW films. (a) XPS spectra of the CNW films before and after electron and proton irradiation. Deconvoluted C 1s peak of the XPS spectra before irradiation (b) and after electron (c) and proton (d) irradiation.

Table 2. Quantitative Analysis of the Chemical Composition of the Surface of the CNW Films

	before irradiation	electron irradiation	proton irradiation
C═C (sp2) (% area)	66.4	68.6	70.4
C−C, C−H (sp3) (% area)	8.8	9.4	11.7
C−OH (% area)	10.0	10.9	10.8
O═C−OH (% area)	14.8	8.1	4.2
O−C═O$^-$ (% area)		3.0	2.9

To evaluate the electronic properties of CNWs before and after the irradiation treatments, the work function was determined using the ultraviolet photoelectron spectroscopy (UPS) technique. Figure 4 shows the UPS spectra of the CNW films before and after the process of electron and proton bombardment. The analysis of the UPS data shows that the value of the work function of the as-prepared reference CNW film is −4.8 eV, which is in good agreement with the literature data.[51,59] After the electron irradiation, this value dropped to −4.76 eV, and after the proton irradiation, the work function decreased even more, down to −4.29 eV. The decrease in work function after the irradiation treatment can be associated with several factors, in particular with a change in the morphological (degree of roughness) and structural properties (orientation of crystals and degree of graphitization) of the material.[60,61] In ref 61, it was reported that the work function of carbon nanostructures decreases with increasing sp^2 content. In our case, the sp^2 content increases after electron and proton irradiation, which is evidenced by the Raman and XPS analysis results.

CNW films have been successfully employed as transparent conductive electrodes in different photodiodes and photodetectors.[62,63] Therefore, the study of the effect of ionizing radiation on the optical properties of CNWs is also of great practical value. In this contribution, we, therefore, also compare the UV−vis transmittance spectra of the CNW films before and after the ionizing radiation treatments (Figure 5). The shape of the measured transmission spectra for the CNW films is very similar to that of graphene sheets.[64,65] Figure 5 indicates that the transmittance of CNW films increases after the electron and proton irradiation. This is expected since the thickness and density of the CNW decrease after the irradiation treatments.

Figure 6 shows the electrical characteristics of CNW films before and after the irradiation treatments. The electrical properties were studied using Hall effect measurements. All electrical characteristics are also presented in Table 3. Figure 6a shows that the sheet resistance of the CNW films increases while the specific conductivity decreases after the irradiation treatments. The sheet resistance of the reference sample is ∼900 Ω/□; after electron irradiation, this value increases by 1.5 times up to ∼1400 Ω/□, and after proton irradiation, the surface resistance increases by 5 times up to ∼4350 Ω/□. The specific electrical conductivity is calculated from the measured sheet resistance and normalized by the film thickness. Specific conductivity represents the electrical properties of the film material itself, which should correlate with the structural and morphological characteristics of the CNW films. The initial value of specific conductivity is ∼70 Ω^{-1} cm^{-1}. After electron irradiation, it drops to ∼45 Ω^{-1} cm^{-1}, whereas after proton irradiation, it drops further down to ∼15 Ω^{-1} cm^{-1}.

Figure 6b shows the measured Hall coefficients of the investigated CNW films. The negative sign of the Hall coefficient (R_H) indicates that all samples before and after irradiation possess n-type conductivity, with electrons as the majority charge carriers. This means that the type of conductivity of the CNW films is immune to ionizing radiation.

https://doi.org/10.1021/acsomega.2c06735
ACS Omega 2022, 7, 48467−48475

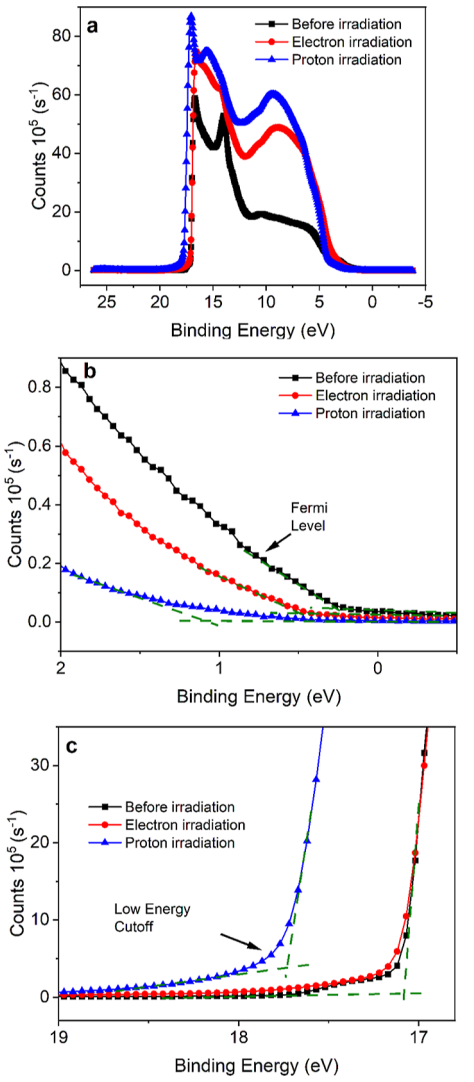

Figure 4. (a) UPS spectra of CNW films before and after electron and proton irradiation. (b) Edge of the UPS spectra, with the Fermi level highlighted. (c) UPS spectra of low-energy cutoff, with the onset highlighted in the graph to determine the work function.

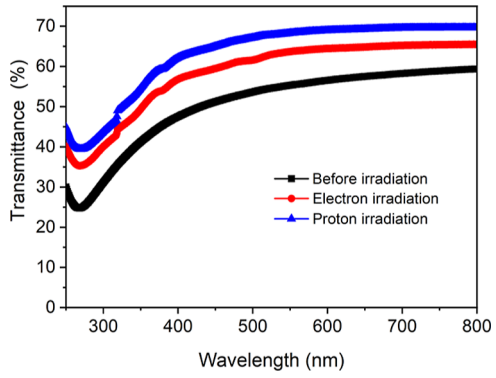

Figure 5. Transmittance of CNW films before and after electron and proton irradiation.

Figure 6c reveals the dependence of the concentration of electrons and their mobility in the CNW films before and after irradiation. The concentration of charge carriers in the as-prepared reference CNW film is 5×10^{18} cm^{-3}; after the electron and proton irradiation treatments, this value increases

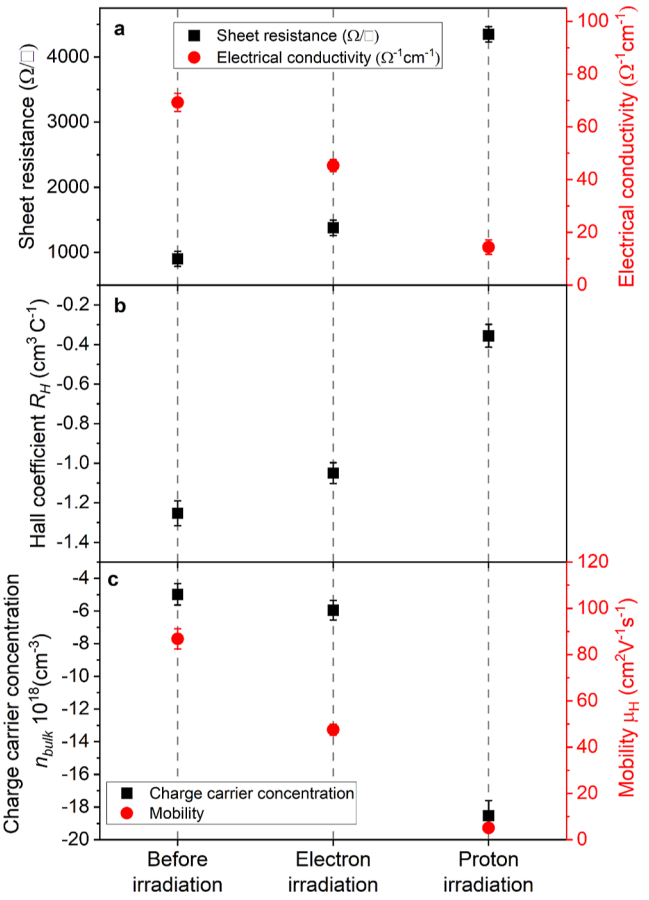

Figure 6. Electrical characteristics of the CNW films before and after electron and proton irradiation. (a) Sheet resistance and specific conductivity. (b) Hall coefficient and (c) charge carrier concentration (negative charge carrier concentration indicates electrons) and mobility.

Table 3. Electrical Characteristics of the CNW Films before and after Electron and Proton Irradiation

electrical characteristics	before irradiation	electron irradiation	proton irradiation
sheet resistance (Ω/□)	902.1	1379.8	4347.8
electrical conductivity (Ω^{-1} cm^{-1})	69.3	45.3	14.4
hall coefficient RH (cm^3 C^{-1})	−1.3	−1.1	−0.4
charge carrier concentration in bulk 10^{18} (cm^{-3})	4.98	5.9	18.5
mobility μH (cm^2 V^{-1} s^{-1})	86.8	47.6	5.1

up to 6×10^{18} and 2×10^{19} cm^{-3}, respectively. The increase in the concentration of charge carriers can be explained by a change in the structural properties of the CNW films after the irradiation treatments, in particular, due to the increase in sp^2 hybridization, which is evidenced by the results of our Raman and XPS analyses.[66,67] It should be mentioned that the increase in the electron concentration is accompanied by a decrease in their mobility after electron and proton bombardments. This phenomenon is most likely also associated with a change in the morphological and structural properties of the irradiated CNWs, as shown earlier in this study.[54,68]

https://doi.org/10.1021/acsomega.2c06735
ACS Omega 2022, 7, 48467−48475

CONCLUSIONS

In conclusion, an integrated approach was applied to study the properties of CNWs and the effect of electron and proton irradiation treatment. The results of this study demonstrate the modification of the morphological and structural properties of the CNW samples depending on the irradiation type. The morphology of CNWs undergoes a significant change, in particular, the wall density decreases after irradiation. Our Raman and XPS analyses independently revealed that the sp^2 hybridization component increases in the CNW films after irradiation. Structural and morphological changes in CNW films after irradiation lead to an alteration in the work function of the material. UPS data analysis shows that the value of the work function of the as-prepared CNW film is −4.8 eV; after electron irradiation, this value shifts to −4.76 eV, and after proton irradiation, the work function decreases to −4.29 eV. The irradiation treatments also lead to changes in the optical and electrical properties of CNWs associated with modifications in their morphology and structural properties. The trend toward an improvement in optical transmission, an increase in surface resistance, and a decrease in the specific conductivity of the CNW films after the irradiation treatments is associated with a decrease in film thickness and CNW density. The obtained results clearly reveal a complex modification of the properties of CNWs after their irradiation with high-energy electrons and protons. However, the change is not very significant, and CNWs themselves still exist on the substrates and remain functional as an optoelectronic material after the irradiation processes. Further experiments to study the effect of irradiation on CNWs should be conducted at different energies of electrons and protons for a better simulation of cosmic conditions. Moreover, a study on the possibility of using these carbon nanostructured films in the development of radiation-resistant optoelectronic devices for space applications is required.

EXPERIMENTAL SECTION

Synthesis of CNW Films. CNW films were synthesized on 1 cm × 1 cm quartz substrates by the inductively coupled plasma chemical vapor deposition (ICP-PECVD) method using methane gas (CH_4) as a carbon source. The quartz substrate was loaded into a CVD furnace with a quartz tube. The quartz tube was pumped down to 10^{-2} Torr and heated up to 800 °C. Then, the CNW films were synthesized at a plasma power of 140 W for 50 min in an Ar/CH_4 and H_2 mixture at flow rates of 20 and 5 cm^3/min, respectively. The experimental setup and the CNW growth mechanism are described in detail in our previous work.[51]

Electron and Proton Irradiation. The ionizing irradiation experiments were conducted in the specialized large-scale facility of the Institute of Nuclear Physics (Almaty, Kazakhstan). Electron irradiation of the samples was carried out at the electron linear accelerator ILU-10 with an electron energy of 5 MeV and a total fluence of 7×10^{13} e/cm^2. The absorbed dose was measured using GEX B6001 polystyrene calorimeters and GEX B3002 film dosimeters based on a Genesys 30 spectrophotometer. Proton irradiation of the samples was carried out at the linear-type cascade rechargeable accelerator UKP 2-1 with a proton energy of 1.5 MeV and a total fluence of 10^{12} p/cm^2. The fluence was determined by measuring the proton beam current using a Digital Current Integrator 439 (ORTEC).

Characterization of the CNW Films. The morphology of the synthesized CNW films was characterized using a scanning electron microscope (SEM, ZEISS Crossbeam 540). A Raman spectrometer (LabRAM HORIBA Evolution and OmegaScope with a laser wavelength of 514.5 nm) was used to study the structural properties of the samples. The electronic properties of the CNW films were characterized using an X-ray photoelectron spectrometer with an Al Kα monochromatic X-ray source at 1486.6 eV (NEXSA, Thermo Scientific) and an ultraviolet photoelectron spectrometer (NEXSA, Thermo Scientific) using a He1α source (21.22 eV). The optical properties of the samples were examined using a UV−vis spectrometer (Lambda 1050, PerkinElmer Ltd.). The electrical properties were studied using a Hall effect measurement system with the van der Pauw configuration (HMS-5500, Ecopia).

AUTHOR INFORMATION

Corresponding Authors

Maratbek T. Gabdullin − *Kazakh-British Technical University, Almaty 050000, Kazakhstan*; Email: gabdullin@physics.kz

Viktor V. Brus − *Department of Physics, Nazarbayev University, Nur-Sultan City 010000, Kazakhstan*; orcid.org/0000-0002-3489-1396; Email: viktor.brus@nu.edu.kz

Authors

Yerassyl Yerlanuly − *Kazakh-British Technical University, Almaty 050000, Kazakhstan; Al-Farabi Kazakh National University, Almaty 050040, Kazakhstan; Department of Physics, Nazarbayev University, Nur-Sultan City 010000, Kazakhstan*; orcid.org/0000-0001-6757-1041

Rakhymzhan Ye Zhumadilov − *Kazakh-British Technical University, Almaty 050000, Kazakhstan; Al-Farabi Kazakh National University, Almaty 050040, Kazakhstan*

Igor V. Danko − *Institute of Nuclear Physics, Almaty 050032, Kazakhstan*; orcid.org/0000-0001-7377-5913

Daniyar M. Janseitov − *Institute of Nuclear Physics, Almaty 050032, Kazakhstan*

Renata R. Nemkayeva − *Kazakh-British Technical University, Almaty 050000, Kazakhstan; Al-Farabi Kazakh National University, Almaty 050040, Kazakhstan*; orcid.org/0000-0002-8782-703X

Alexander V. Kireyev − *Institute of Nuclear Physics, Almaty 050032, Kazakhstan*

Aidana B. Arystan − *Kazakh-British Technical University, Almaty 050000, Kazakhstan*

Gulnur Akhtanova − *Department of Physics, Nazarbayev University, Nur-Sultan City 010000, Kazakhstan*

Joachim Vollbrecht − *Institut für Solarenergieforschung GmbH, Emmerthal 31860, Germany*

Nora Schopp − *University of California Santa Barbara, Santa Barbara, California 93106, United States*; orcid.org/0000-0002-6920-0241

Aliya Nurmukhanbetova − *Energetic Cosmos Laboratory, Nazarbayev University, Nur-Sultan City 010000, Kazakhstan*

Tlekkabul S. Ramazanov − *Al-Farabi Kazakh National University, Almaty 050040, Kazakhstan*

Askhat N. Jumabekov − *Department of Physics, Nazarbayev University, Nur-Sultan City 010000, Kazakhstan*; orcid.org/0000-0003-0051-9542

https://doi.org/10.1021/acsomega.2c06735
ACS Omega 2022, 7, 48467−48475

Pavel A. Oreshkin − *Institute of Nuclear Physics, Almaty 050032, Kazakhstan*
Timur K. Zholdybayev − *Institute of Nuclear Physics, Almaty 050032, Kazakhstan*

Complete contact information is available at: https://pubs.acs.org/10.1021/acsomega.2c06735

Author Contributions

Y.Y.: investigation, formal analysis, methodology, visualization, validation, writing—original draft, and writing—review and editing. R.Y.Z.: investigation. I.V.D.: resources, investigation. D.M.J.: investigation. R.R.N.: investigation, formal analysis, visualization, writing—original draft. A.V.K.: investigation. A.B.A.: formal analysis, visualization. G.A.: visualization, investigation. J.V.: methodology, writing—review & editing. N. S.: methodology, writing—review & editing. A.N.: resources, investigation. T.S.R.: methodology. A.N.J.: resources, methodology. P.A.O.: resources, methodology. T.K.Z.: resources, investigation. M.T.G.: project administration, funding acquisition. V.V.B.: conceptualization, methodology, supervision, funding acquisition, writing—review & editing.

Notes

The authors declare no competing financial interest.

■ ACKNOWLEDGMENTS

We would like to thank the Core Facilities team of Nazarbayev University for the help and support with XPS, UPS, and SEM measurements and Aslan Samarkanov for graphic abstract. V.V.B. thanks the Nazarbayev University Collaborative Research Grant (grant number: 11022021CRP1505) and the Nazarbayev University Faculty Development Competitive Research Grant (grant number: 11022021FD2915). A.N.J. thanks the Nazarbayev University Collaborative Research Grant (grant number: 021220CRP1922). M.T.G. thanks the Scientific Research Grant from the Science Committee of the Ministry of Education and Science of the Republic of Kazakhstan (grant no. AP08856684).

■ REFERENCES

(1) Guérin, Y.; Was, G. S.; Zinkle, S. J. Abstract References Materials Challenges for Advanced Nuclear Energy Systems. *MRS Bull.* **2009**, *34*, 10−14.
(2) Zhang, Y.; Weber, W. J. Ion Irradiation and Modification: The Role of Coupled Electronic and Nuclear Energy Dissipation and Subsequent Nonequilibrium Processes in Materials. *Appl. Phys. Rev.* **2020**, *7*, 041307.
(3) Kanhaiya, P. S.; Yu, A.; Netzer, R.; Kemp, W.; Doyle, D.; Shulaker, M. M. Carbon Nanotubes for Radiation-Tolerant Electronics. *ACS Nano* **2021**, *15*, 17310−17318.
(4) Kirmani, A. R.; Durant, B. K.; Grandidier, J.; Haegel, N. M.; Kelzenberg, M. D.; Lao, Y. M.; McGehee, M. D.; McMillon-Brown, L.; Ostrowski, D. P.; Peshek, T. J.; Rout, B.; Sellers, I. R.; Steger, M.; Walker, D.; Wilt, D. M.; VanSant, K. T.; Luther, J. M. Countdown to Perovskite Space Launch: Guidelines to Performing Relevant Radiation-Hardness Experiments. *Joule* **2022**, *6*, 1015−1031.
(5) Nwankwo, V. U. J.; Kio, N. T.; Michael, T. *The Impact of Space Radiation Environment on Satellites Operation in Near-Earth Space. Satellites Missions and Technologies for Geosciences*; IntechOpen, 2020.
(6) Lubin, P.; Cohen, A. N.; Erlikhman, J. Radiation Effects from the Interstellar Medium and Cosmic Ray Particle Impacts on Relativistic Spacecraft. *Astrophys. J.* **2022**, *932*, 134.
(7) Brown, C. R.; Whiteside, V. R.; Poplavskyy, D.; Hossain, K.; Dhoubhadel, M. S.; Sellers, I. R. Flexible Cu(In,Ga)Se$_{2}$ Solar Cells for Outer Planetary Missions: Investigation Under Low-Intensity Low-Temperature Conditions. *IEEE J. Photovoltaics* **2019**, *9*, 552−558.
(8) Krasheninnikov, A. V.; Nordlund, K. Ion and Electron Irradiation-Induced Effects in Nanostructured Materials. *J. Appl. Phys.* **2010**, *107*, 071301.
(9) Pan, C.-T.; Hinks, J. A.; Ramasse, Q. M.; Greaves, G.; Bangert, U.; Donnelly, S. E.; Haigh, S. J. In-Situ Observation and Atomic Resolution Imaging of the Ion Irradiation Induced Amorphisation of Graphene. *Sci. Rep.* **2015**, *4*, 6334.
(10) Yitzhak, N. M.; Girshevitz, O.; Haran, A.; Butenko, A.; Kaveh, M.; Shlimak, I. Evidence of Structural Changes in Ion-Irradiated Graphene Independent of the Incident Ions Mass. *Appl. Surf. Sci.* **2022**, *597*, 153701.
(11) Brus, V. V.; Solovan, M. M.; Schopp, N.; Kaikanov, M.; Mostovyi, A. I. Visible to Near-Infrared Photodiodes with Advanced Radiation Resistance. *Adv. Theory Simul.* **2022**, *5*, 2100436.
(12) Hudson, A.; Hubbard, S.; Juang, B.-C.; Liang, B.; Debnath, M.; Lotshaw, W. Electron Radiation Effects on Carrier Relaxation in Molecular Beam and Vapor Deposition Grown GaAs Test Structures. *J. Appl. Phys.* **2022**, *131*, 075703.
(13) Chandra, S.; Das, P.; Bag, S.; Laha, D.; Pramanik, P. S. Functionalization and Bioimaging Applications of Highly Fluorescent Carbon Nanoparticles. *Nanoscale* **2011**, *3*, 1533.
(14) Wang, Z.; Shen, D.; Wu, C.; Gu, S. State-of-the-Art on the Production and Application of Carbon Nanomaterials from Biomass. *Green Chem.* **2018**, *20*, 5031−5057.
(15) Peng, Z.; Liu, X.; Zhang, W.; Zeng, Z.; Liu, Z.; Zhang, C.; Liu, Y.; Shao, B.; Liang, Q.; Tang, W.; Yuan, X. Advances in the Application, Toxicity and Degradation of Carbon Nanomaterials in Environment: A Review. *Environ. Int.* **2020**, *134*, 105298.
(16) He, Y.; Hu, C.; Li, Z.; Wu, C.; Zeng, Y.; Peng, C. Multifunctional Carbon Nanomaterials for Diagnostic Applications in Infectious Diseases and Tumors. *Mater. Today Bio* **2022**, *14*, 100231.
(17) Bertolo, A. A.; Cánneva, A.; Donadelli, J. A.; Gaviola, P. A.; Kreiner, A. J.; del Grosso, M. F. Manufacture, Characterization and Proton Irradiation Effects of $$\hat{}{12}\hbox {C}$$ and $$\hat{}{13}\hbox {C}$$ Thick Targets. *J. Mater. Sci.* **2021**, *56*, 6997−7007.
(18) Shi, T.; Peng, Q.; Bai, Z.; Gao, F.; Jovanovic, I. Proton Irradiation of Graphene: Insights from Atomistic Modeling. *Nanoscale* **2019**, *11*, 20754−20765.
(19) Wang, W.; Wang, S.; Zhang, S.; Wang, W.; Ji, X.; Li, C. Effects of Substrates on Proton Irradiation Damage of Graphene. *RSC Adv.* **2020**, *10*, 12060−12067.
(20) Jagodar, A.; Berndt, J.; von Wahl, E.; Strunskus, T.; Lecas, T.; Kovacevic, E.; Brault, P. Nitrogen Incorporation in Graphene Nanowalls via Plasma Processes: Experiments and Simulations. *Appl. Surf. Sci.* **2022**, *591*, 153165.
(21) Narayan, J.; Joshi, P.; Smith, J.; Gao, W.; Weber, W. J.; Narayan, R. J. Q-Carbon as a New Radiation-Resistant Material. *Carbon* **2022**, *186*, 253−261.
(22) de Campos da Costa, J. P.; Teodoro, V.; Assis, M.; Bettini, J.; Andrés, J.; Pereira do Carmo, J. P.; Longo, E. A Scalable Electron Beam Irradiation Platform Applied for Allotropic Carbon Transformation. *Carbon* **2021**, *174*, 567−580.
(23) Vatankhah, A. R.; Hosseini, M. A.; Malekie, S. The Characterization of Gamma-Irradiated Carbon-Nanostructured Materials Carried out Using a Multi-Analytical Approach Including Raman Spectroscopy. *Appl. Surf. Sci.* **2019**, *488*, 671−680.
(24) Peng, B.; Locascio, M.; Zapol, P.; Li, S.; Mielke, S. L.; Schatz, G. C.; Espinosa, H. D. Measurements of Near-Ultimate Strength for Multiwalled Carbon Nanotubes and Irradiation-Induced Crosslinking Improvements. *Nat. Nanotechnol.* **2008**, *3*, 626−631.
(25) Simos, N.; Hurh, P.; Mokhov, N.; Snead, M.; Topsakal, M.; Palmer, M.; Ghose, S.; Zhong, H.; Kotsina, Z.; Sprouster, D. J. Low-Temperature Proton Irradiation Damage of Isotropic Nuclear Grade IG-430 Graphite. *J. Nucl. Mater.* **2020**, *542*, 152438.

(26) Wu, Y.; Qiao, P.; Chong, T.; Shen, Z. Carbon Nanowalls Grown by Microwave Plasma Enhanced Chemical Vapor Deposition. *Adv. Mater.* **2002**, *14*, 64−67.
(27) Yerlanuly, Y.; Christy, D.; Van Nong, N.; Kondo, H.; Alpysbayeva, B.; Nemkayeva, R.; Kadyr, M.; Ramazanov, T.; Gabdullin, M.; Batryshev, D.; Hori, M. Synthesis of Carbon Nanowalls on the Surface of Nanoporous Alumina Membranes by RI-PECVD Method. *Appl. Surf. Sci.* **2020**, *523*, 146533.
(28) Kurita, S.; Yoshimura, A.; Kawamoto, H.; Uchida, T.; Kojima, K.; Tachibana, M.; Molina-Morales, P.; Nakai, H. Raman Spectra of Carbon Nanowalls Grown by Plasma-Enhanced Chemical Vapor Deposition. *J. Appl. Phys.* **2005**, *97*, 104320.
(29) Ichikawa, T.; Shimizu, N.; Ishikawa, K.; Hiramatsu, M.; Hori, M. Synthesis of Isolated Carbon Nanowalls via High-Voltage Nanosecond Pulses in Conjunction with CH4/H2 Plasma Enhanced Chemical Vapor Deposition. *Carbon* **2020**, *161*, 403−412.
(30) Davami, K.; Shaygan, M.; Kheirabi, N.; Zhao, J.; Kovalenko, D. A.; Rümmeli, M. H.; Opitz, J.; Cuniberti, G.; Lee, J.-S.; Meyyappan, M. Synthesis and Characterization of Carbon Nanowalls on Different Substrates by Radio Frequency Plasma Enhanced Chemical Vapor Deposition. *Carbon* **2014**, *72*, 372−380.
(31) Vesel, A.; Zaplotnik, R.; Primc, G.; Mozetič, M. Synthesis of Vertically Oriented Graphene Sheets or Carbon Nanowalls—Review and Challenges. *Materials* **2019**, *12*, 2968.
(32) Hiramatsu, M.; Shiji, K.; Amano, H.; Hori, M. Fabrication of Vertically Aligned Carbon Nanowalls Using Capacitively Coupled Plasma-Enhanced Chemical Vapor Deposition Assisted by Hydrogen Radical Injection. *Appl. Phys. Lett.* **2004**, *84*, 4708−4710.
(33) Kawai, S.; Kondo, S.; Takeuchi, W.; Kondo, H.; Hiramatsu, M.; Hori, M. Optical Properties of Evolutionary Grown Layers of Carbon Nanowalls Analyzed by Spectroscopic Ellipsometry. *Jpn. J. Appl. Phys.* **2010**, *49*, 060220.
(34) Yang, C.; Bi, H.; Wan, D.; Huang, F.; Xie, X.; Jiang, M. Direct PECVD Growth of Vertically Erected Graphene Walls on Dielectric Substrates as Excellent Multifunctional Electrodes. *J. Mater. Chem. A* **2013**, *1*, 770−775.
(35) Liu, J.; Sun, W.; Wei, D.; Song, X.; Jiao, T.; He, S.; Zhang, W.; Du, C. Direct Growth of Graphene Nanowalls on the Crystalline Silicon for Solar Cells. *Appl. Phys. Lett.* **2015**, *106*, 043904.
(36) Lin, G.; Zhou, Y.; Wang, Y.; Yan, X.; Wu, B.; Huang, F.; Fu, J.; Cheng, Q.; Yun, D. Direct Growth of Graphene Nanowalls on Quartz Substrates as Transparent Conductive Electrodes for Perovskite Solar Cells. *Funct. Mater. Lett.* **2018**, *11*, 1850009.
(37) Wei, W.; Sun, K.; Hu, Y. H. Synthesis of Mesochannel Carbon Nanowall Material from CO_2 and Its Excellent Performance for Perovskite Solar Cells. *Ind. Eng. Chem. Res.* **2017**, *56*, 1803−1809.
(38) Han, T.-H.; Lee, Y.; Choi, M.-R.; Woo, S.-H.; Bae, S.-H.; Hong, B. H.; Ahn, J.-H.; Lee, T.-W. Extremely Efficient Flexible Organic Light-Emitting Diodes with Modified Graphene Anode. *Nat. Photonics* **2012**, *6*, 105−110.
(39) Ci, H.; Chang, H.; Wang, R.; Wei, T.; Wang, Y.; Chen, Z.; Sun, Y.; Dou, Z.; Liu, Z.; Li, J.; Gao, P.; Liu, Z. Enhancement of Heat Dissipation in Ultraviolet Light-Emitting Diodes by a Vertically Oriented Graphene Nanowall Buffer Layer. *Adv. Mater.* **2019**, *31*, 1901624.
(40) Seo, D. H.; Pineda, S.; Fang, J.; Gozukara, Y.; Yick, S.; Bendavid, A.; Lam, S. K. H.; Murdock, A. T.; Murphy, A. B.; Han, Z. J.; Ostrikov, K. Single-Step Ambient-Air Synthesis of Graphene from Renewable Precursors as Electrochemical Genosensor. *Nat. Commun.* **2017**, *8*, 14217.
(41) Tomatsu, M.; Hiramatsu, M.; Foord, J. S.; Kondo, H.; Ishikawa, K.; Sekine, M.; Takeda, K.; Hori, M. Hydrogen Peroxide Sensor Based on Carbon Nanowalls Grown by Plasma-Enhanced Chemical Vapor Deposition. *Jpn. J. Appl. Phys.* **2017**, *56*, 06HF03.
(42) Watanabe, H.; Kondo, H.; Sekine, M.; Hiramatsu, M.; Hori, M. Control of Super Hydrophobic and Super Hydrophilic Surfaces of Carbon Nanowalls Using Atmospheric Pressure Plasma Treatments. *Jpn. J. Appl. Phys.* **2012**, *51*, 01AJ07.
(43) Gao, J. M.; Song, X. F.; Hu, J.; Guo, S. C.; Fang, L.; Wu, F.; Wei, D. P. Superhydrophobic Graphenic Carbon Nanowalls Fabricated by One-Step PECVD. *Mater. Lett.* **2016**, *184*, 273−277.
(44) Chi, Y.-W.; Hu, C.-C.; Shen, H.-H.; Huang, K.-P. New Approach for High-Voltage Electrical Double-Layer Capacitors Using Vertical Graphene Nanowalls with and without Nitrogen Doping. *Nano Lett.* **2016**, *16*, 5719−5727.
(45) Bo, Z.; Zhu, W.; Ma, W.; Wen, Z.; Shuai, X.; Chen, J.; Yan, J.; Wang, Z.; Cen, K.; Feng, X. Vertically Oriented Graphene Bridging Active-Layer/Current-Collector Interface for Ultrahigh Rate Supercapacitors. *Adv. Mater.* **2013**, *25*, 5799−5806.
(46) Yi, F.; Ren, H.; Shan, J.; Sun, X.; Wei, D.; Liu, Z. Wearable Energy Sources Based on 2D Materials. *Chem. Soc. Rev.* **2018**, *47*, 3152−3188.
(47) Zamarayeva, A. M.; Ostfeld, A. E.; Wang, M.; Duey, J. K.; Deckman, I.; Lechêne, B. P.; Davies, G.; Steingart, D. A.; Arias, A. C. Flexible and Stretchable Power Sources for Wearable Electronics. *Sci. Adv.* **2017**, *3*, No. e1602051.
(48) Esquinazi, P.; Spemann, D.; Schindler, K.; Höhne, R.; Ziese, M.; Setzer, A.; Han, K.-H.; Petriconi, S.; Diaconu, M.; Schmidt, H.; Butz, T.; Wu, Y. H. Proton Irradiation Effects and Magnetic Order in Carbon Structures. *Thin Solid Films* **2006**, *505*, 85−89.
(49) Hou, L.; Chen, Z.; Zhao, Z.; Sun, X.; Zhang, J.; Yuan, C. Universal $FeCl_3$ -Activating Strategy for Green and Scalable Fabrication of Sustainable Biomass-Derived Hierarchical Porous Nitrogen-Doped Carbons for Electrochemical Supercapacitors. *ACS Appl. Energy Mater.* **2019**, *2*, 548−557.
(50) Sun, Z.; Liu, Y.; Ye, W.; Zhang, J.; Wang, Y.; Lin, Y.; Hou, L.; Wang, M.; Yuan, C. Unveiling Intrinsic Potassium Storage Behaviors of Hierarchical Nano Bi@N-Doped Carbon Nanocages Framework via In Situ Characterizations. *Angew. Chem., Int. Ed.* **2021**, *60*, 7180−7187.
(51) Yerlanuly, Y.; Zhumadilov, R.; Nemkayeva, R.; Uzakbaiuly, B.; Beisenbayev, A. R.; Bakenov, Z.; Ramazanov, T.; Gabdullin, M.; Ng, A.; Brus, V. V.; Jumabekov, A. N. Physical Properties of Carbon Nanowalls Synthesized by the ICP-PECVD Method vs. the Growth Time. *Sci. Rep.* **2021**, *11*, 19287.
(52) Malard, L. M.; Pimenta, M. A.; Dresselhaus, G.; Dresselhaus, M. S. Raman Spectroscopy in Graphene. *Phys. Rep.* **2009**, *473*, 51−87.
(53) Johns, S.; Poulsen, T.; Kane, J. J.; Windes, W. E.; Ubic, R.; Karthik, C. Formation of Carbon Nanostructures in Nuclear Graphite under High-Temperature in Situ Electron-Irradiation. *Carbon* **2019**, *143*, 908−914.
(54) Cho, H. J.; Kondo, H.; Ishikawa, K.; Sekine, M.; Hiramatsu, M.; Hori, M. Density Control of Carbon Nanowalls Grown by CH4/H2 Plasma and Their Electrical Properties. *Carbon* **2014**, *68*, 380−388.
(55) Lesiak, B.; Kövér, L.; Tóth, J.; Zemek, J.; Jiricek, P.; Kromka, A.; Rangam, N. C. Sp2/Sp3 in Carbon Nanomaterials − XPS and (X)AES Study. *Appl. Surf. Sci.* **2018**, *452*, 223−231.
(56) Biesinger, M. C. Accessing the Robustness of Adventitious Carbon for Charge Referencing (Correction) Purposes in XPS Analysis: Insights from a Multi-User Facility Data Review. *Appl. Surf. Sci.* **2022**, *597*, 153681.
(57) Morais, A.; Alves, J. P. C.; Lima, F. A. S.; Lira-Cantu, M.; Nogueira, A. F. Enhanced Photovoltaic Performance of Inverted Hybrid Bulk-Heterojunction Solar Cells Using TiO 2/Reduced Graphene Oxide Films as Electron Transport Layers. *J. Photon. Energy* **2015**, *5*, 057408.
(58) Dementyev, P.; Naberezhnyi, D.; Westphal, M.; Buck, M.; Gölzhäuser, A. Carbon Nanomembranes from Aromatic Carboxylate Precursors. *ChemPhysChem* **2020**, *21*, 1006−1011.
(59) Shimada, S.; Teii, K.; Nakashima, M. Low Threshold Field Emission from Nitrogen-Incorporated Carbon Nanowalls. *Diamond Relat. Mater.* **2010**, *19*, 956−959.
(60) Naghdi, S.; Sanchez-Arriaga, G.; Rhee, K. Y. Tuning the Work Function of Graphene toward Application as Anode and Cathode. *J. Alloys Compd.* **2019**, *805*, 1117−1134.
(61) Lin, Y.; Feng, Z.; Yu, L.; Gu, Q.; Wu, S.; Su, D. S. Insights into the Surface Chemistry and Electronic Properties of Sp^2 and Sp^3

https://doi.org/10.1021/acsomega.2c06735
ACS Omega 2022, 7, 48467−48475

-Hybridized Nanocarbon Materials for Catalysis. *Chem. Commun.* **2017**, *53*, 4834−4837.
(62) Liu, X.; Zhou, Q.; Luo, S.; Du, H.; Cao, Z.; Peng, X.; Feng, W.; Shen, J.; Wei, D. Infrared Photodetector Based on the Photothermionic Effect of Graphene-Nanowall/Silicon Heterojunction. *ACS Appl. Mater. Interfaces* **2019**, *11*, 17663−17669.
(63) Shen, J.; Liu, X.; Song, X.; Li, X.; Wang, J.; Zhou, Q.; Luo, S.; Feng, W.; Wei, X.; Lu, S.; Feng, S.; Du, C.; Wang, Y.; Shi, H.; Wei, D. High-Performance Schottky Heterojunction Photodetector with Directly Grown Graphene Nanowalls as Electrodes. *Nanoscale* **2017**, *9*, 6020−6025.
(64) Lee, H. C.; Liu, W.-W.; Chai, S.-P.; Mohamed, A. R.; Aziz, A.; Khe, C.-S.; Hidayah, N. M. S.; Hashim, U. Review of the Synthesis, Transfer, Characterization and Growth Mechanisms of Single and Multilayer Graphene. *RSC Adv.* **2017**, *7*, 15644−15693.
(65) Xu, S. C.; Man, B. Y.; Jiang, S. Z.; Chen, C. S.; Yang, C.; Liu, M.; Gao, X. G.; Sun, Z. C.; Zhang, C. Direct Synthesis of Graphene on SiO2 Substrates by Chemical Vapor Deposition. *CrystEngComm* **2013**, *15*, 1840.
(66) Rosenburg, F.; Balke, B.; Nicoloso, N.; Riedel, R.; Ionescu, E. Effect of the Content and Ordering of the Sp2 Free Carbon Phase on the Charge Carrier Transport in Polymer-Derived Silicon Oxycarbides. *Molecules* **2020**, *25*, 5919.
(67) Kim, K. J.; Eom, J.-H.; Koh, T. Y.; Kim, Y.-W.; Seo, W.-S. Effects of Carbon Addition on the Electrical Properties of Bulk Silicon-Oxycarbide Ceramics. *J. Eur. Ceram. Soc.* **2016**, *36*, 2705−2711.
(68) Takeuchi, W.; Ura, M.; Hiramatsu, M.; Tokuda, Y.; Kano, H.; Hori, M. Electrical Conduction Control of Carbon Nanowalls. *Appl. Phys. Lett.* **2008**, *92*, 213103.

https://doi.org/10.1021/acsomega.2c06735
ACS Omega 2022, 7, 48467−48475